# Fusion Research and International Collaboration in the Asian Region*⁾

Shigeru MORITA, Liqun HU[1], Yeong-Kook OH[2], Naoko ASHIKAWA, Mitsutaka ISOBE,
Daiji KATO, Yasuaki KISHIMOTO[3], Satoshi OHDACHI, Satoru SAKAKIBARA,
Yasushi TODO, Yutaka KAMADA[4], Daniel RAJU[5] and Min XU[6]

*National Institute for Fusion Science, Toki, Gifu 509-5292, Japan*
[1]*Institute of Plasma Physics, Chinese Academy of Sciences, Hefei, Anhui 230031, China*
[2]*National Fusion Research Institute, Daejeon 34133, Korea*
[3]*Graduate School of Energy Science, Kyoto University, Uji, Kyoto 611-0011, Japan*
[4]*National Institutes for Quantum and Radiological Science and Technology (QST), Chiba 263-8555, Japan*
[5]*Institute for Plasma Research, Bhat, Gandhinagar 382428, India*
[6]*Southwestern Institute of Physics, P. O. Box 432, Chengdu 610041, China*

In recent years, fusion research has become exceedingly popular in the Asian region. Many toroidal devices are currently operated for fusion research in universities and institutes. The long pulse operation of a high-performance plasma is also possible in four superconducting devices, which are EAST (Institute of Plasma Physics Chinese Academy of Sciences (ASIPP), China), KSTAR (National Fusion Research Institute (NFRI), Korea), LHD (National Institute for Fusion Science (NIFS), Japan) and SST-1 (Institute for Plasma Research (IPR), India). The world's largest superconducting tokamak, JT-60SA (National Institutes for Quantum and Radiological Science and Technology (QST), Japan), and middle-size tokamak, HL-2 M (Southwestern Institute of Physics (SWIP), China), have now been constructed for the upcoming operation. Based on the progressive development of fusion research in Asian region an international collaboration on critical physics for the steady state operation of high-performance plasmas has been carried out among China, Japan and Korea during past five years through the A3 foresight program. Recent fusion research activities in the Asian region and the results of the collaboration are briefly reported with future prospects for international collaboration.

## 1. Introduction

Recently, fusion research activities in Asian region have been steadily spreading to many countries and regions. However, international collaboration has not comprehensively developed in this region, except for local collaborations, such as that between KSTAR and JT-60, while several international fusion programs are being conducted in the world. To address this situation, three institutes, which are the Institute of Plasma Physics, Chinese Academy of Science (ASIPP, China), National Fusion Research Institute (NFRI, Korea), and National Institute for Fusion Science (NIFS, Japan) have initiated the A3 foresight program [1] in 2012 under the auspices of The National Natural Science Foundation of China (NSFC, China), The Japan Society for the Promotion of Science (JSPS, Japan), and the National Research Foundation of Korea (NRF, Korea). The A3 program with a history of five years of collaboration during 2012–2017 basically comprises joint experiments among three superconducting fusion devices of EAST, KSTAR, and LHD in specific fields for steady state sustainment of high-performance plasmas. The fostering of young scientists, including PhD students is also an important subject. The results of the A3 program collaboration are reported with a brief introduction on the recent status of the currently existing and upcoming fusion devices in Asian region. In addition, future prospects for further enhancement of international collaboration in Asian region are briefly summarized.

## 2. Present Status of Fusion Research in the Asian Region

### 2.1 Superconducting devices

At present, four superconducting toroidal devices of EAST (ASIPP, China) [2], KSTAR (NFRI, Korea) [3], LHD (NIFS, Japan) [4], and the SST-1 (Institute for Plasma Research: IPR, India) [5] which are listed in Table 1 have been operated in the Asian region for the feasibility study on steady state sustainment of high-

performance plasmas.

In EAST, a stationary 400 s H-mode and 1000 s long pulse discharge at tungsten divertor configuration are aimed at mission research based on the non-inductive current drive. The long pulse discharge in EAST is non-inductively sustained by a lower-hybrid wave current drive (LHCD) [6]. A strong Li-coating is performed to reduce edge particle recycling and to increase edge electron temperature. The LHCD efficiency is considerably improved with enhancements of non-thermal electron confinement and plasma rotation, while the reason for this improvement is unclear. Consequently, high-density LHCD discharges are possible at $f_{LHCD} = 4.6$ GHz, e.g., $3 \times 10^{13}$ cm$^{-3}$. The lower-hybrid wave (LHW) can also contribute to edge localized mode (ELM) mitigation in the upper single-null discharges with a tungsten divertor configuration as well as a resonant magnetic perturbation (RMP) field. At present, a 101 s H-mode LHCD discharge is achieved at $n_e = 3 \times 10^{13}$ cm$^{-3}$ by suppressing tungsten accumulation. During the discharge, the tungsten divertor temperature is also sustained below 600°C.

In KSTAR, a steadily high $\beta_N$ ($\beta_N \leq 4$) discharge of up to 300 s is aimed by injecting tangential neutral beams. The installation of a tungsten divertor and advanced current drive, e.g., a high-field side LHCD, are also scheduled in KSTAR as a reactor-mode study, while the present experiment is being carried out for a carbon divertor and first wall. Although a full non-inductive operation of up to 20 s has already been obtained with the LHCD in KSTAR [7], the long pulse discharge with high-performance plasma has been attempted with a long pulse neutral-beam injection (NBI). At present, a 70 s long pulse H-mode discharge with $P_{NBI} = 4$ MW and $P_{ECH} = 0.8$ MW is achieved at $n_e = 3 \times 10^{13}$ cm$^{-3}$, $\beta_N \sim 2.0$ and $\beta_P \sim 2.5$. However, the plasma performance, e.g., $T_e(0)$ and $\beta_N$, gradually decreases during the long pulse discharge with increased wall recycling and $V_{loop}$. To keep the wall recycling lower during the long pulse NBI discharge, a high-temperature wall discharge at 150°C has been initiated from the 2017 experimental campaign. On the other hand, in KSTAR, a remarkable result has been obtained on the ELM-crash suppression. The ELM activity is suppressed by ITER-like three row $n = 1$ RMP coils during 34 s.

In SST-1, superconducting toroidal field coils have been routinely operated at $B_t = 1.5$ T with a discharge length limited to the half second. Then, enhancement of the $B_t$ and extension of the discharge length will be attempted in the upcoming experiments for further improvement of the discharge performance.

Unlike tokamak, LHD is characterized by a current-less plasma discharge, the steady sustainment of which is relatively easier. In addition, LHD has several unique characters, e.g., the presence of a fully three-dimensional (3-D) edge stochastic magnetic field layer and a steadily quiescent magnetic island formation, which can provide an excellent tool for plasma physics. Instead of hydrogen discharges which have been carried out for the past 20 years, deuterium experiments have been initiated in the LHD on March 2017. The performance characteristics of the deuterium plasma are now being studied in comparison with those of the hydrogen plasma. In LHD, until now, an hour long pulse ICRF (ion cyclotron range of frequency) discharge with $P_{ICRF} = 0.4$ MW is achieved at $n_e = 0.4 \times 10^{13}$ cm$^{-3}$ and $T_e(0) \sim T_i(0) \sim 1$ keV with the help of ECH (electron cyclotron heating, $P_{ECH} = 0.1$ MW) [8]. During the steady discharge, the magnetic axis position, $R_{ax}$, is periodically swung in the range of $3.65 \leq R_{ax} \leq 3.67$ m to change the divertor strike points. Consequently, the divertor temperature is successfully maintained below 300°C. A steady operation of the detached plasma during 4 s is also achieved in LHD using $n/m = 1/1$ RMP coils, while the duration of the detached plasma is limited by the pulse length of NBI.

## 2.2 Normal conducting devices

There are many normal conducting toroidal devices, including small devices in university laboratories in the East Asian region. Several medium-sized ($R \sim 1$ m) toroidal devices are operated in EAST Asian region, i.e., QUEST [9] in Kyushu Univ. (Japan), Heliotron-J [10] in Kyoto Univ. (Japan), J-TEXT [11] in Huazhong Univ. of Sci. and Tech. (China), and KTX [12] in Univ. of Sci. and Tech. of China, where studies are mainly carried out on current startup for spherical torus, basic experiments for alternative helical device concept, diagnostics development, and development of alternative magnetic configuration using reversed field pinch, respectively. In particular, in HL-2A [13] at Southwestern Institute of Physics (SWIP, China) listed in Table 1, several unique studies based on the normal conducting tokamak have been carried out on turbulence, zonal flow, H-mode physics, energetic particle driven MHD (magnetohydrodynamics), and impurity transport.

Many tokamak experiments have been also carried out in the West Asian region. Table 1 lists the typical three tokamaks. MHD studies, including current disruption and mode locking and basic spherical tokamak experiments are being carried out in IR-T1 (Islamic Azad Univ., Iran) [14] and GLAST (National Tokamak Fusion Program, Pakistan) [15], respectively. In KTM tokamak (Institute of Atomic Energy Branch of National Nuclear Center, Kazakhstan) [16] for material study, a liquid lithium divertor experiment is planned in the near future.

## 2.3 Devices under construction

In the East Asian region, on the other hand, two tokamaks of HL-2 M (SWIP) [17] and JT-60SA (National Institutes for Quantum and Radiological Science and Technology: QST, Japan) [18] are now being constructed for an upcoming operation (see Table 1). The main aim for operating the HL-2 M normal conducting tokamak is to

Table 1 Designed machine parameters and start of operation.

| Device | $R/a$(m) | $B_t$(T) | $I_p$(MA) | $\kappa/\delta$ | operation |
|---|---|---|---|---|---|
| LHD (J)* | 3.6/0.64 | 3 | | 1.8/0.9** | 1998 |
| EAST (C) | 1.7/0.4 | 3.5 | 1.0 | 2.0/0.5 | 2006 |
| KSTAR (K) | 1.8/0.5 | 3.5 | 2.0 | 2.0/0.8 | 2008 |
| SST-1 (I) | 1.1/0.2 | 3 | 0.22 | 2/0.7 | 2013 |
| HL-2A (C) | 1.65/0.4 | 2.2 | 2.5 | 1.3/0.3 | 2002 |
| | | (3.0) | (3.0)*** | | |
| KTM (Ka) | 0.86/0.43 | 1 | 0.75 | 1.7/- | --- |
| IR-T1 (Ir) | 0.45/0.13 | 0.9 | 0.06 | limiter | 1995 |
| GLAST (P) | 0.15/0.09 | 0.4 | 0.05 | 2.5/- | --- |
| HL-2M (C) | 1.78/0.65 | 2.2 | 2.5 | 2/0.5 | upcoming |
| JT-60SA (JE) | 2.97/1.18 | 2.25 | 5.5 | 1.93/0.5 | 2020 |

*J: Japan, C: China, K: Korea, I: India, Ka: Kazakhstan, Ir: Iran, P: Pakistan, JE: Japan & EU joint research
**Diameters at long/short axes of elliptical plasma cross section
***Values in brackets are design parameters

obtain experimental outputs to support International Thermonuclear Experimental Reactor (ITER) [19] and China Fusion Engineering Test Reactor (CFETR) [20] through physics studies related to burning plasma and divertor. JT-60SA, typically characterized by a high $\beta_N$ and $f_{BS}$, is the world's largest, highly shaped superconducting tokamak and its plasma size is about half of ITER. The main mission of operating JT-60SA is to make a contribution to an early realization of fusion energy utilization by addressing key physics and engineering issues for ITER and Demonstration Fusion Power Reactor (DEMO). For this purpose, a 100 s long pulse discharge with break-even-equivalent class high-performance deuterium plasmas is scheduled based on 100 s 34 MW NBI (24 MW for 85 keV p-NBI (positive-ion-source-based NBI) and 10 MW for 500 keV n-NBI (negative-ion-source-based NBI)) and 7 MW ECH (110 and 138 GHz) heating. Of course, the fostering of young scientists using JT-60SA is also an important objective for the continuation of active fusion research in ITER and DEMO.

# 3. Results of the A3 Foresight Program

As shown in Fig. 1, there are many physics and engineering requirements for the construction of a fusion reactor. The sustainment of the reactor plasma is also one such requirement. When a discharge is longer, the handling of high heat load over the divertor and the first wall surrounding high-temperature plasma becomes a vital issue because it creates an entirely different situation from what has been studied in normal conducting toroidal devices with the discharge length strictly limited. The study of critical physics for the steady state operation of high-performance plasma has been made possible only by superconducting devices
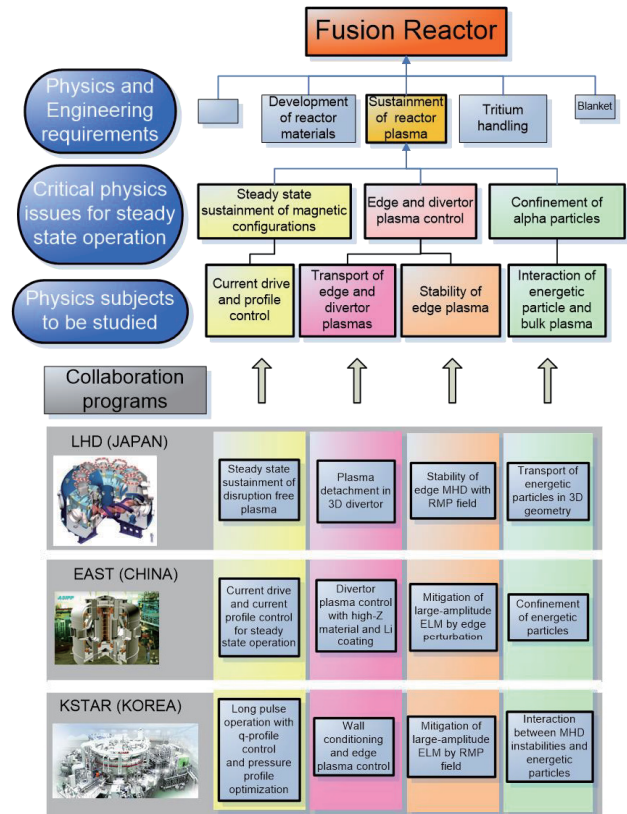


Fig. 1 Schematic drawing on Joint Research Project among LHD, EAST and KSTAR. Engineering requirements for the reactor can be reduced through collaborative studies on critical physics issues specific to steady state discharges of high-performance plasma. The Joint Research Project quests three critical physics issues for the steady state operation and these issues consist of four key physics subjects to be studied.

of EAST, KSTAR, and LHD. The following three categories based on the critical physics issues for steady state operation are then listed up for the A3 foresight program, primarily among the three devices.

(I) Steady state sustainment of magnetic configuration
(II) Edge and divertor plasma control
 (IIa) Transport of edge and divertor plasmas
 (IIb) Stability of edge plasma
(III) Confinement of alpha particles
(IV) Theory and simulation for (I) - (III)

## 3.1 Steady state discharge sustainment

The characteristic time scale of energy and particle transports in high-temperature plasmas is of the order of the energy confinement time, e.g., $0.1 \sim 1$ s, in existing large tokamaks and the LHD. On the other hand, the magnetic configuration formed by an external magnetic field and plasma itself evolves along with the time scale of magnetic diffusion time, e.g., $\leq 50$ s in existing devices and $\sim 200$ s in ITER, that is, the MHD equilibrium evolution takes much longer than the plasma does in the existing

tokamaks. Therefore, for the realization of an attractive fusion reactor, it is crucial whether the high-performance plasma can be sustained for a longer period than the magnetic diffusion time, while high-performance plasmas are sustained only transiently in existing tokamaks. In addition, for a tokamak, the toroidal plasma current has to be steadily sustained using non-inductive current drives and self-generated current called bootstrap current, while for a helical device, the plasma can be sustained without such help. Of course, heat load mitigation/removal in the divertor region is also an important issue for the steady discharge sustainment. Then, in Category I, collaborative works among EAST, KSTAR, and LHD are focused on studies of steady state operation.

### 3.1.1 Long pulse discharges

Efforts for achieving longer pulse operation with high-performance plasmas have been made continuously in the three devices. Recent results on the long pulse operation have been described already in section 2.1. Here, we want to emphasize the difference in the technologies among the three devices to maintain the long pulse operation, i.e., the LHCD in EAST, the NBI in KSTAR, and the ICRF in LHD. These entirely different approaches toward the long pulse discharge can bring us a variety of knowledges in getting over several problems that occur in the discharge trial. These knowledges certainly contribute to the ITER operation.

### 3.1.2 Current profile control

By controlling the plasma current profile or safety factor (q) profile, internal transport barrier (ITB) formation in core plasmas can be achieved. In particular, because the bootstrap current can reduce the requirement for a non-inductive current drive, it is important to study the bootstrap current. Since the plasma pressure is relatively low in the long pulse discharge of EAST, the plasma current by the LHCD reaches 75 %, while the bootstrap current is 22 % [21]. In EAST, then, the current profile can be controlled by changing the density by which radial penetration and deposition of the LHW are affected, and resultantly by modifying a profile of non-thermal electrons carrying the plasma current. Thus, a broader current profile is obtained with the off-axis LHCD. Recently in the KSTAR, ITB formation was found during a plasma current ramp-up phase before the appearance of the H-mode [22]. Typical ITB structures are observed in ion and toroidal rotation profiles. In addition, the current profile control is planned to obtain broader current and pressure profiles by installing an off-axis tangential NBI. In the LHD, on the other hand, the rotational transform profile, $\iota(\rho)$ ($\equiv 1/q(\rho)$), does not relate to the plasma production, while deformation of the $\iota(\rho)$ due to an increased plasma pressure enhances stability through formation of a magnetic well region in the plasma core.

### 3.1.3 Dust during long pulse discharges

Because dust frequently disturbs the extension of the long pulse discharge, the study of dust is now one of the critical issues to achieve steady state operation.

In LHD, large amount of dusts from the divertor region are observed with fast framing cameras before the plasma termination during a long pulse discharge [23, 24]. An arcing is triggered at a small gap between the stainless steel armor tiles on the first wall. The long pulse discharge is terminated with an abrupt increase in iron influx. In EAST, tungsten dust often drops from the upper tungsten divertor during H-mode discharges [25]. If the dust size is large, the discharge is terminated after 50 ms of the tungsten dust drop due to a quickly increasing radiation loss. In KSTAR, then, the dust particle is quantitatively examined using a fast framing camera [26]. It is found that the dust consists of various shapes of broken graphite pieces, stainless steel, copper, and so on, e.g., circle, ellipse and flake. The size of these dusts ranges between 0.43 and 1701 $\mu m^2$ with a peak size of 2 $\mu m^2$. The average flux and total weight are found to be 3.5 particles $\cdot cm^2 s^{-1}$ and 9.6 mg/day, respectively. A method for controlling the dust during the long pulse discharge has to be explored intensively to ensure steady state operation.

## 3.2 Transport of edge and divertor plasmas
### 3.2.1 Impurity transport

Collaborative works in Category IIa on impurity transport have been done using LHD, EAST, and the HL-2A. For this purpose, several vacuum ultraviolet (VUV) and extreme ultraviolet (EUV) spectrometers have been installed on EAST [27] and HL-2A [28, 29] to measure temporal behavior and radial profiles of impurity line emissions at 50 - 500 Å. In LHD, on the other hand, two-dimensional (2-D) EUV spectroscopy at 50 - 500 Å [30] has also been developed in addition to the radial profile measurement at 10 - 130 Å [31]. The results of the collaboration are briefly summarized in the following.

#### 3.2.1.1 Edge impurity transport

Carbon transport in the scrape-off layer (SOL) of HL-2A, where the parallel transport is dominant, is studied for different impurity source locations such as limiter, dome and divertor [32]. Radial profiles of CIII and CIV clearly vary with different source locations, i.e., a flat carbon emission profile from the divertor source, slightly peaked profile from the dome source, and a peaked profile from the limiter source. The results are analyzed with a 3-D edge plasma transport code, EMC3-EIRENE. The simulation strongly suggests that a poloidal asymmetry of the impurity flow and an enhanced physical sputtering sufficiently affect the impurity profile in the SOL, indicating an important role in carbon screening in the SOL.

In LHD, carbon transport is studied in attached and RMP-assisted detached plasmas based on vertical profile

and 2-D distribution measurements [33–35]. It is found that the CIII and CIV emissions in the stochastic magnetic field layer, where both parallel and cross-field transports are important due to long magnetic field connection length, $L_c$, are drastically enhanced in the vicinity of the island O-point and both edge separatrix X-points during the RMP-assisted detachment, thereby suggesting a change in the magnetic field structure. On the contrary, the CVI emission located radially inside the magnetic island is significantly reduced, suggesting an increase in the impurity screening during the detachment. The cross-field transport of $C^{3+}$ ions, $D_{Z\perp}$, in the stochastic magnetic field layer has been investigated with EMC3-EIRENE. Consequently, it has been found that the $D_{Z\perp}$ is 20 times larger than that of bulk ions. The impurity screening effect of iron ions in the presence of a stochastic magnetic field layer has also been studied [36]. Recently, a close relation between the edge impurity flow and friction force along magnetic fields was experimentally certificated for the first time in LHD [37].

### 3.2.1.2 Core impurity transport

Core impurity transport in the outer half of the plasma radius is studied in low-density ECH discharges ($2 \times 10^{13}$ cm$^{-3}$) of HL-2A [38]. A ratio of CV to CIV indicating an index of the core impurity transport between LCFS (last closed flux surface) and a radial region of the CV emission, e.g. $\rho = 0.6$, is measured with a space-resolved VUV spectrometer. The result shows a gradual decrease against $n_e$ in ohmic discharges, while the ratio suddenly decreases just after turning off the ECH. The CIV and CV radial profiles are analyzed with a transport code. It is found that, during the ECH phase, the radial convection of $C^{4+}$ ions changes from inward to outward. However, in the ohmic discharge, it is always an inward convection. Since the neoclassical impurity outward flux due to temperature and density gradients is relatively small, trapped electron mode (TEM) driven turbulent transport and an effect of positive electric field during ECH are discussed. In LHD, it is found that the density of iron ions with higher collisionality at hollow $n_e$ profiles is much smaller than that at peaked $n_e$ profiles [39]. A simulation code analysis strongly suggests that an impurity transport barrier is formed in the hollow $n_e$ profile based on a neoclassical effect on the ion density gradient. In EAST, it is found that the confinement of metallic impurities can be reduced by LHW heating [40].

### 3.2.1.3 Suppression of tungsten accumulation

Suppression of tungsten accumulation has been studied in EAST with tungsten divertor configuration. In particular, the study is important for NBI H-mode discharges because the impurity accumulation frequently occurs in such discharges. The tungsten behavior is investigated by measuring tungsten unresolved transition array (W-UTA) at 45 - 70, which is composed of several ionization stages of tungsten, e.g., $W^{27+} - W^{45+}$ at $T_e \sim 2.5$ keV. It is found that the tungsten accumulation occurring during the

H-mode phase can be suppressed when LHW (4.6 GHz, $P_{LHW} = 0.8$ MW) is superposed on the NBI discharge [41]. In addition, it is found that the tungsten density measured with W-UTA largely depends on the power ratio of $P_{LHW}/(P_{LHW} + P_{NBI})$ and can be reduced by an order of magnitude of $P_{LHW}/(P_{LHW} + P_{NBI}) \geq 0.8$. In addition to the LHW, effects of ECH and RMP field are also being studied for tungsten suppression.

### 3.2.2 Plasma wall interaction

For the PWI study in Category IIa, common tungsten specimens have been used during the collaboration. The tungsten specimens are exposed to KSTAR and EAST discharges with different plasma conditions, and then the surface analysis of the exposed specimens is mainly carried out in Japan and China.

#### 3.2.2.1 Deuterium retention of tungsten and molybdenum

Deuterium retention on the tungsten sample after plasma exposure has been studied by Kyushu Univ. and Lanzhou Chemical Institute. By measuring the depth profile, it is found that the surface is characterized by three tungsten deposition layers. Microcrystalline structures are observed in the tungsten deposition layer using transmission electron spectroscopy. It is revealed that the microcrystalline structure enhances the deuterium retention in comparison with the crystallized structure [42, 43].

The deuterium retention has also been studied during an ion cyclotron resonance frequency wall conditioning (ICWC) in EAST. It is found that an influence of the hydrogen isotope exchange in the tungsten sample extends to a depth of 30 nm [44].

Deuterium depth profiles in lithium-coated layer on the tungsten specimen have been studied in two different conditions, i.e., short period plasma exposure during morning lithium wall conditioning and long period plasma exposure during an experimental campaign in 2016. In the short exposure, a 0.4 μm thick lithium-coated layer is observed with a 0.2 μm depth deuterium retention; in the long exposure, a 7 μm thick lithium-coated layer is observed with deeply distributed deuterium retention. Here, it should be noted that the plasma facing components are entirely coated by lithium at the beginning of the experimental campaign in EAST [45].

Molybdenum specimens exposed to deuterium plasmas in KSTAR have been analyzed by measuring the deuterium depth profile. The deuterium retention at strike points in the divertor region is lower than that at the plasma peripheral region. Therefore, it is revealed that the deuterium deposited in the molybdenum specimen is diffused and finally released by a temperature increase during a long pulse discharge of 18 seconds [45].

#### 3.2.2.2 Deuterium recycling

A density decay time, which is measured from den-

sity decay after turning off the deuterium gas feed, has been investigated in EAST to study wall recycling. The results are compared between low and high power LHCD discharges with an upper single-null configuration. The resultant density reduction analyzed at the exponential decay is found to be $1.1 \times 10^{13}\,\mathrm{cm}^{-3}$ at $P_{\mathrm{LHCD}} = 600\,\mathrm{kW}$ and $0.8 \times 10^{13}\,\mathrm{cm}^{-3}$ at $P_{\mathrm{LHCD}} = 1800\,\mathrm{kW}$. The large recycling observed at higher power may suggest an influence of suprathermal electrons driven by LHCD. In addition, the deuterium recycling is studied by comparing the density decay between initial and final discharges of the day. The density decay time in the final shot is a few times longer than that in the initial shot, indicating a clear effect of enhanced wall recycling due to the shot accumulation.

### 3.2.3 Atomic and molecular processes

Tungsten spectra have been studied in Category IIa for edge plasma diagnostics of ITER. The studies are carried out on the theoretical explanations of quasi-continuum emissions called UTA consisting of many emission lines in different ionization stages, in addition to observations of EUV and visible spectra from CoBIT (compact electron beam trap) and LHD. A collisional-radiative (CR) model based on detailed atomic processes is used for analysis of the tungsten line spectrum. Validation of the CR model is important for an accurate explanation of the tungsten EUV spectrum that is experimentally observed from highly ionized tungsten ions.

#### 3.2.3.1 Tungsten spectra in EUV region

The CoBIT [46, 47] can confine highly ionized ions by axially supplying an electrostatic potential well at the central drift tube. The ionization stage of trapped ions is successively increased by a mono-energetic electron beam through collisional ionization. Therefore, spectra from tungsten ions in a single ionization stage can be easily observed from the CoBIT, while the tungsten spectrum from fusion plasmas is complicated due to superposition of different temperature regions along the observation chord. Since the electron density in CoBIT is very low, e.g., $10^{10}\,\mathrm{cm}^3$ which is three orders of magnitude smaller than that in fusion plasmas, the tungsten spectrum is formed only through an electron impact excitation from the ground state. It means the tungsten spectrum from the CoBIT can be easily understood through a common knowledge. Tungsten EUV spectra from LHD plasmas have therefore been attempted to explain using simple spectra from CoBIT in NIFS [48]. Consequently, the LHD tungsten UTA spectrum in 15 - 35 Å can be well explained by the CoBIT spectrum synthesized at two different electron beam energies of 0.95 and 1.37 keV, since 6g-4f and 5g-4f transitions and 5f-4d and 5p-4d transitions forming the UTA spectrum are dominant at the two energies in CoBIT.

A CR model is developed to explain the tungsten UTA spectrum from LHD plasmas [49]. The CoBIT UTA spectrum is also used for the validation of the CR model. The

CR model calculates level populations at 23,000 J-resolved fine-structures with a principal quantum number of up to 6 for a single ion. An effect of the inner-shell excitation is newly considered in the model. Hence, the UTA spectrum simulated with the CR model at 15 - 30 Å and 40 - 70 Å is in good agreement with the LHD spectrum. Recently, the UTA spectrum has been experimentally examined well in LHD by measuring a radial profile [50]. It has been found that wavelength intervals of 49.2 - 49.46 Å, 48.81 - 49.03 Å, and 47.94 - 48.15 Å, at which the spectrum consists of a single ionization stage of $W^{27+}$, $W^{26+}$ and $W^{24+}$, respectively, are applicable to the tungsten diagnostic.

#### 3.2.3.2 Tungsten M1 spectra in visible region

Any neutron damage on the spectroscopic instrument can be avoided by using optical fibers, when visible emissions are available for tungsten diagnostics. At present, the visible line applicable for tungsten measurement is practically limited to only neutral tungsten atoms. On the contrary, it is known that the wavelength of magnetic-dipole (M1) lines among 4f ground states of highly ionized tungsten ions falls into the UV-visible range and the transition probability becomes quickly larger with the atomic number. Based on the physics background favorable to the tungsten ion, several M1 lines have been recently found for $W^{7+}$, $W^{13+}$ and $W^{26-28+}$ ions using CoBIT, in particular, at University of Electro-Communications [51, 52] (Japan) and Fudan University (China) [53,54]. State-of-the-art theoretical atomic structure calculation [55] agrees with the measured wavelength within a few percent. The M1 line of highly ionized tungsten ions is also observed in the UV-visible range in LHD [56,57], which has been observed for the first time in fusion plasmas. The tungsten ion density in the core region of the LHD plasma is now being analyzed using the measured M1 lines [58].

## 3.3 Stability of edge plasma

The control of edge instabilities caused by a steep pressure gradient is one of the critical issues in current fusion research to steadily sustain the high-performance plasma. For example, a heat flux on the divertor plate induced by a specific ELM, e.g., type-I ELM, is hazardous for a next-generation tokamak such as ITER. Therefore, it is urgent to find a proper way to control edge MHD activities. At present, it is believed that an external application of the RMP field is the most promising way to mitigate the giant ELM, while the physical reason why the RMP can affect the MHD activity has not been fully understood. In Category IIb, then, three subjects are implemented toward understanding of the RMP physics.

### 3.3.1 Evaluation of equilibrium during RMP

Knowledge on the equilibrium magnetic field is essentially important in discussing the stability of edge MHD activities. A deformation of the equilibrium during RMP

has been evaluated using a HINT code for several devices, e.g., LHD and HL-2A. To observe the deformation of edge magnetic surfaces directly, 2-D SX (soft x-ray) and VUV camera systems have been jointly developed to be installed on KSTAR. Stocastization of the edge magnetic field by RMP is also investigated in KSTAR using the radial propagation of the heat pulse triggered by a sawtooth crash [59]. A transitional change from nested magnetic surface to stochastic magnetic fields is experimentally evidenced deep inside the LCFS, based on the radial profile analysis of the heat pulse propagation.

### 3.3.2 Visualization of edge MHD activities

Since the edge localized mode has a large mode number, an imaging diagnostic is one of the possible ways to visualize the edge MHD activity because ELMs are generally accompanied by large mode numbers. A VUV camera system for the imaging diagnostic is developed as a collaborative work in EAST to visualize the edge MHD activity during the H-mode phase with ELMs [60]. In addition, the collaboration is done in HL-2A by installing a SX camera system on a tangential port to enhance the signal intensity. To initiate imaging data analysis in the near future, the detector system and signal quality are now being checked.

### 3.3.3 Control of edge MHD activities using RMP

Suppression of the resistive interchange mode ($m/n = 2/3$ and $1/2$) is succeeded in LHD when the RMP with $m/n = 1/1$ is externally supplied [61]. As shown in Fig. 2, when the RMP coil current is increased, the amplitude of $m/n = 2/3$ and $2/4$ MHD modes is reduced. As seen in Fig. 2 (a), the pressure gradient at a rational surface where

the mode exists is unchanged, even if the RMP coil current changes. This may suggest that a transitional change in the magnetic field topology can stabilize the MHD activity directly, i.e., the resistive interchange mode. Understanding of the RMP physics on the MHD activity has progressed significantly through the joint research between LHD and tokamaks.

## 3.4 Interaction of energetic particle and bulk plasma

Confinement of energetic particles (EP) is one of the crucial issues in magnetic confinement fusion, since 3.5 MeV alpha particles produced by D-T reactions play an essential role in the achievement of self-ignition in future burning plasmas. A comparative study on the EP confinement between tokamak and helical devices are absolutely necessary for a comprehensive understanding of the EP-related physics in toroidal systems. As the first step in Category III, then, efforts are made on the development of a standard instrument for the EP diagnostic.

### 3.4.1 FILD and neutron detector systems

Since a scintillator-based fast-ion loss detector (FILD) has been developed in CHS and LHD over the years [62], the FILD developed in NIFS is adopted as a standard instrument for the collaborative work. As a result of close joint works, as shown in Fig. 3, the FILD has been successfully installed on four devices of LHD [63], KSTAR [64], HL-2A [65] and EAST [66, 67]. Based on the common detector system, effects of RMP fields and MHD instabilities on EP behavior are studied in detail in LHD, KSTAR and HL-2A [68–70]. In addition, the characteristics on a prompt loss of the energetic ion arising from a neutral beam for additional heating are studied in KSTAR [71]. Long-lived runaway electrons during a major disruption are also investigated in HL-2A to study the production and growth mechanism [72].

On the other hand, in neutral-beam heated deuterium plasmas, the neutron yield is dominated by a beam-plasma reaction. Therefore, the neutron diagnostic can also be used for diagnostics of the energetic particle. A standard
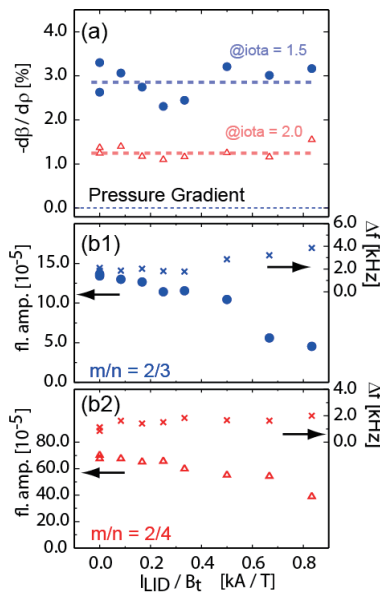


Fig. 2 (a) Pressure gradient and mode amplitudes of (b1) $m/n = 2/3$ and (b2) $m/n = 2/4$ activities as a function of RMP fields. Widths of frequency spectra in MHD activities are also shown at right vertical axis in (b1) and (b2).
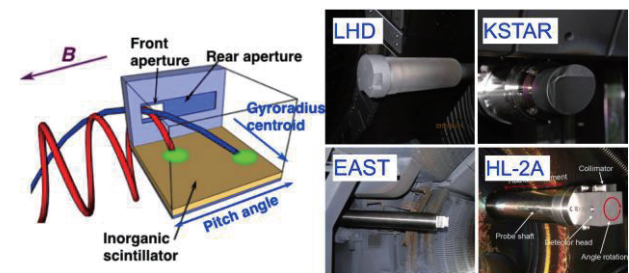


Fig. 3 Orbits of escaping energetic particles in FILD (left) and photographs of FILD installed on four toroidal devices (right). The FILD simultaneously provides information on energy and pitch angle of escaping energetic particles.

detector system for the neutron diagnostic has been installed on LHD, KSTAR, EAST, and HL-2A. A neutron profile monitor has been also developed in HL-2A as a collaborative work [73]. The slowing-down process of the beam ion is studied in HL-2A by measuring a decay rate of the neutron emission after an NB blip. The result indicates that the tangentially injected beam ions follow a classical slowing-down process without significant loss [74], whereas a beam ion loss occurs in discharges where MHD instabilities such as tearing mode and beta-induced Alfvén acoustic eigenmodes are destabilized [75].

### 3.4.2 Triton burnup ratio

Recently, a remarkable progress has been made on the triton burnup study. A confinement property of 1 MeV tritons produced by D(D, p)T reaction is investigated in LHD [76, 77] and KSTAR [78] using a neutron activation system (NAS) [79]. Since kinematic parameters of the 1 MeV triton, e.g., Larmor radius and drift frequency, are quite similar to those of 3.5 MeV alpha particles, the 1 MeV triton can be used as a test particle for confinement simulation of the alpha particle. The triton yields 14 MeV neutrons through a secondary D-T reaction during the energy decay process. Then, a triton burnup ratio is defined as a yield ratio of D-T 14 MeV neutrons to D-D 2.5 MeV neutrons. The burnup ratio measured with NAS in KSTAR and LHD is shown in Fig. 4. In KSTAR, the ratio increases with $I_p$ as expected because a banana orbit width becomes narrower with $I_p$. The maximum ratio of 0.48 % is obtained at $I_p = 0.83$ MA. In LHD, this ratio increases when



Fig. 4   Triton burnup ratio in KSTAR [75] and LHD.

the magnetic axis position, $R_{ax}$, is inwardly shifted. This occurs due to a confinement improvement of the helically trapped triton at smaller $R_{ax}$. The maximum ratio observed in LHD is quite similar to the KSTAR tokamak, i.e., 0.45 % at $R_{ax} = 3.55$ m.

## 3.5 Theory and simulation

Collaborative works in Category IV on theory and simulation studies consist of the following three subjects which are important for the steady state sustainment of high-performance plasmas.

### 3.5.1 Confinement of energetic particles

The confinement of energetic particles and MHD instabilities driven by energetic particles are studied in EAST and KSTAR using a hybrid simulation code called MEGA, which has been developed at NIFS for a study of energetic particles interacting with an MHD fluid [80]. The simulation is carried out with realistic equilibrium data constructed by using the EFIT code. Three dominant fast-ion-driven modes in EAST plasmas, i.e., toroidicity-induced Alfvén eigenmodes, reversed shear Alfvén eigenmodes and energetic particle modes, are identified in the simulation [81]. It is found that the shearing profile of Alfvén eigenmodes can be induced by a non-perturbative effect of the fast ion. Fishbone instabilities are also investigated in EAST using the MEGA code [82]. Nonlinear frequency chirping-down and nonlinear dynamics of resonant particles are clarified with the simulation. For passing particles, the resonance remains within the $q = 1$ surface, while, for trapped particles, the resonant location radially moves out during the nonlinear evolution. The MEGA code is also applied to the Alfvén eigenmode study in KSTAR [83].

### 3.5.2 Physical properties of peripheral plasmas

Collaboration is carried out between NIFS and ASIPP by developing a 1-D particle-in-cell simulation (PIC) code, and then, 2-D PIC code (PIC2) is developed for the study of EAST plasmas. Based on the PIC2 code, particle and heat fluxes onto the EAST divertor plate are studied. For 3-D fluid simulations of the EAST and LHD peripheral plasmas, a computational program for the grid construction is being completed through the collaborative work between NIFS and DUT (Dalian Univ. of Tech., China). The first result on the EAST peripheral plasma is obtained for tungsten divertor discharges [84]. Analysis is also done for the stochastic magnetic layer of LHD [35, 85]

### 3.5.3 Multi-scale turbulence

Based on collaborative works on the multi-scale turbulence simulation between Kyoto Univ. and DUT, it is revealed that macroscopic MHD tearing mode and microscopic ion-temperature-gradient turbulence can mutually destabilize each other [86]. Generation dynamics and structural characteristics of zonal flows are also investi-
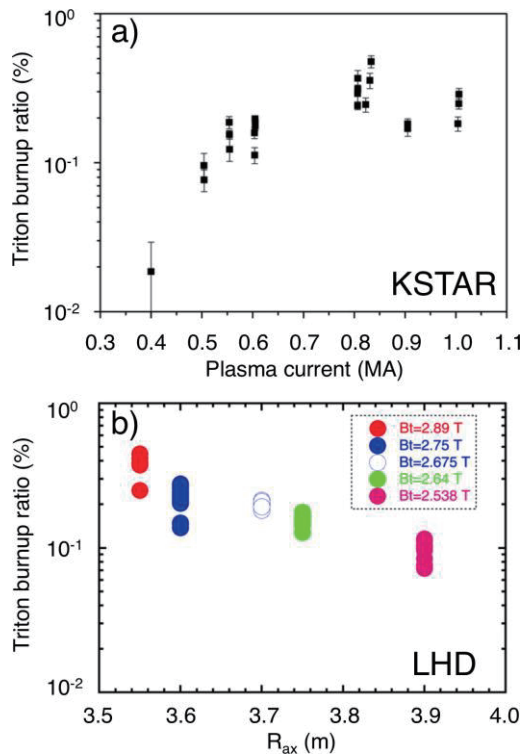
gated in the double tearing mode with antisymmetric shear flows. Two types of zonal flow oscillations are found in the reduced resistive MHD simulation [87]. A nonlinear evolution of the Kelvin-Helmholtz instability driven by a radially antisymmetric shear flow in the double current sheet configuration is numerically investigated based on a reduced MHD model [88]. In addition, momentum transport, nonlocal transport phenomena, and ITB formation are studied as collaborative works among Kyoto Univ., NFRI, and SWIP.

# 4. Future Prospects for International Collaboration

Based on the A3 program, 600 personal exchanges, which include many PhD students, have been carried out between China, Japan and Korea during the past five years. A3 seminars have also been held 15 times, successively rotating among the three countries, and the seminar proceedings have been summarized in the NIFS-PROC series [89–101]. More than 100 papers have been published in scientific journals with peer review as a result of international collaborations and 9 invited talks have been presented at international conferences. However, the education of overseas PhD students in the Asian region is highly localized in Japan. Further exchange of overseas PhD students in the Asian region is strongly encouraged to enhance future fusion research activity.

At present, in the Asian region, several toroidal devices are planned for construction. In China, in particular, a design study related to a stellarator device, CFQS (Chinese First Quasi-axisymmetric Stellarator), has been initiated toward its construction in Southwest Jiatong University in China. The study is aimed at a reduced neoclassical transport and an improved particle orbit. The initiation of stellarator research in China has resulted in the international collaboration in the Asian region becoming closer and deeper. In addition, new stellarator and tokamak programs have also been initiated in University of South China in Hengyang and Chiang Mai University in Thailand, respectively. These new programs have promisingly enhanced the personal exchange of PhD students and young scientists in the Asian region.

# Acknowledgments

[1] http://www.jsps.go.jp/j-foresight/01_boshuyoko.html
[2] B.N. Wan *et al.*, Nucl. Fusion **57**, 102019 (2017).
[3] Y.-K. Oh *et al.*, Proc. 26th IAEA Fusion Energy Conf. (17-22 Oct., 2016, Kyoto, Japan) OV/2-4.
[4] Y. Takeiri *et al.*, Nucl. Fusion **57**, 102023 (2017).
[5] S. Pradhan *et al.*, Nucl. Fusion **55**, 104009 (2015).
[6] B.J. Ding *et al.*, Nucl. Fusion **53**, 113027 (2013).
[7] J.G. Kwak *et al.*, Nucl. Fusion **53**, 104005 (2013).
[8] T. Mutoh *et al.*, Nucl. Fusion **53**, 063017 (2013).
[9] K. Hanada *et al.*, Plasma Fusion Res. **5**, S1007 (2010).
[10] T. Obiki *et al.*, Nucl. Fusion **44**, 47 (2004).
[11] G. Zhuang *et al.*, Nucl. Fusion **57**, 102003 (2017).
[12] W.D. Liu *et al.*, Nucl. Fusion **57**, 116038 (2017).
[13] X.R. Duan *et al.*, Nucl. Fusion **57**, 102013 (2017).
[14] R. Alipour *et al.*, Eur. Phys. J. D **71**, 60 (2017).
[15] Z. Ahmad *et al.*, Phys. Scr. **92**, 045601 (2017).
[16] I. Lyublinski *et al.*, Fusion Eng. Des. **87**, 1719 (2012).
[17] D.Q. Liu *et al.*, Fusion Eng. Des. **96-97**, 298 (2015).
[18] H. Shirai *et al.*, Nucl. Fusion **57**, 102002 (2017).
[19] J.A. Snipes *et al.*, Nucl. Fusion **57**, 125001 (2017).
[20] Y.X. Wan *et al.*, Nucl. Fusion **57**, 102009 (2017).
[21] F.K. Liu *et al.*, Nucl. Fusion **55**, 123022 (2015).
[22] J. Chung *et al.*, Nucl. Fusion **58**, 016019 (2018).
[23] M. Shoji *et al.*, Nucl. Fusion **55**, 053014 (2015).
[24] M. Shoji *et al.*, Nucl. Mater. Energy **12**, 779 (2017).
[25] L. Zhang *et al.*, ITC26/APFA-11 (5-8 Dec., 2017, Toki, Japan) O-2.
[26] A. Autricque *et al.*, Nucl. Mater. Energy **12**, 599 (2017).
[27] L. Zhang *et al.*, Rev. Sci. Instrum. **86**, 123509 (2015).
[28] H.Y. Zhou *et al.*, Rev. Sci. Instrum. **83**, 10D507 (2012).
[29] Z.Y. Cui *et al.*, Rev. Sci. Instrum. **85**, 11E426 (2014).
[30] H.M. Zhang *et al.*, Jpn. J. Appl. Phys. **54**, 086101 (2015).
[31] X.L. Huang *et al.*, Rev. Sci. Instrum. **85**, 043511 (2014).
[32] Z.Y. Cui *et al.*, Nucl. Fusion **55**, 093034 (2015).
[33] S. Morita *et al.*, Plasma Phys. Control. Fusion **56**, 094007 (2014).
[34] H.M. Zhang *et al.*, Phys. Plasmas **24**, 022510 (2017).
[35] S.Y. Dai *et al.*, Nucl. Fusion **56**, 066005 (2016).
[36] S. Morita *et al.*, Nucl. Fusion **53**, 093017 (2013).
[37] T. Oishi *et al.*, Nucl. Fusion **58**, 016040 (2018).
[38] Z.Y. Cui *et al.*, Nucl. Fusion **53**, 093001 (2013).
[39] X.L. Huang *et al.*, Nucl. Fusion **57**, 086031 (2017).
[40] Z. Xu *et al.*, Nucl. Fusion **58**, 016001 (2018).
[41] L. Zhang *et al.*, Nucl. Mater. Energy **12**, 774 (2017).
[42] K. Katayama *et al.*, Nucl. Mater. Energy **12**, 617 (2017).
[43] N. Ashikawa *et al.*, 18th Int. Conf. Fusion Reactor Mater. (6-11 Nov., 2017, Aomori, Japan) 7PT32.
[44] N. Ashikawa *et al.*, 13th China-Japan Symposium on Mater. (26-29 Sep., 2016, Hefei, China).
[45] N. Ashikawa *et al.*, ITC26/APFA-11 (5-8 Dec., 2017, Toki, Japan) O-1.
[46] N. Nakamura *et al.*, Rev. Sci. Instrum. **79**, 063104 (2008).
[47] H.A. Sakaue *et al.*, Phys. Rev. A **92**, 012504 (2015).
[48] S. Morita *et al.*, AIP Conf. Proc. **1545**, 143 (2013).
[49] I. Murakami *et al.*, Nucl. Fusion **55**, 093016 (2015).
[50] Y. Liu *et al.*, J. Appl. Phys. **122**, 233301 (2017).
[51] M. Mita *et al.*, Atoms **5**, 13 (2017).
[52] Y. Kobayashi *et al.*, Phys. Rev. A **92**, 022510 (2015).
[53] M. Qiu *et al.*, J. Phys. B. **47**, 175002 (2014).
[54] Z. Fei *et al.*, Phys. Rev. A **86**, 062501 (2012).
[55] X.B. Ding *et al.*, J. Phys. B **44**, 145004 (2012); Phys. Lett. A **380**, 874 (2016).
[56] D. Kato *et al.*, Phys. Scr. **T156**, 014081 (2013).
[57] K. Fujii *et al.*, J. Phys. B **50**, 055004 (2017).

[58] D. Kato *et al.*, Proc. 26th IAEA Fusion Energy Conf. (17-22 Oct., 2016, Kyoto, Japan) EX/P8-14.

[59] S. Ohdachi *et al.*, NIFS-PROC-98 (2015).

[60] Z.J. Wang *et al.*, Plasma Sci. Technol. **20**, 025103 (2018).

[61] S. Ohdachi *et al.*, Nucl. Fusion **55**, 093006 (2016).

[62] M. Isobe *et al.*, Rev. Sci. Instrum. **70**, 827 (1999).

[63] J. Kim *et al.*, Rev. Sci. Instrum. **83**, 10D305 (2012).

[64] Y.P. Zhang *et al.*, Rev. Sci. Instrum. **85**, 053502 (2014).

[65] J.F. Chang *et al.*, Rev. Sci. Instrum. **87**, 11E728 (2016).

[66] Z. Jin *et al.*, Fusion Eng. Des. **125**, 160 (2017).

[67] M. Isobe *et al.*, Fusion Sci. Technol. **72**, 60 (2017).

[68] K. Ogawa *et al.*, Nucl. Fusion **53** 053012 (2013).

[69] K. Ogawa *et al.*, Plasma Phys. Control. Fusion **56**, 094005 (2014).

[70] Y.P. Zhang *et al.*, Nucl. Fusion **55**, 113024 (2015).

[71] J. Young Kim *et al.*, AIP Advances **6**, 105013 (2016).

[72] Y.P. Zhang *et al.*, Phys. Plasmas **19**, 032510 (2012).

[73] Y.P. Zhang *et al.*, Rev. Sci. Instrum. **87**, 063503 (2016).

[74] Y.P. Zhang *et al.*, Phys. Plasmas **19**, 112504 (2012).

[75] Y. Liu *et al.*, Nucl. Fusion **52**, 074008 (2012).

[76] M. Isobe *et al.*, submitted to IEEE Trans. Plasma Sci.

[77] K. Ogawa *et al.*, to be published in Nuclear Fusion.

[78] J. Jo *et al.*, Rev. Sci. Instrum. **87**, 11D828 (2016).

[79] N. Pu *et al.*, Rev. Sci. Instrum. **88**, 113302 (2017).

[80] Y. Todo and T. Sato, Phys. Plasmas **5**, 1321 (1998).

[81] Y. Hu *et al.*, Phys. Plasmas **23**, 022505 (2016).

[82] Y. Pei *et al.*, Phys. Plasmas **24**, 032507 (2017).

[83] T. Rhee *et al.*, 11th Asian Pacific Plasma Theory Conf. (1-4 July, 2014, Jeju, Korea).

[84] S.Y. Dai *et al.*, 11th A3 seminar (11 - 14 July, 2017, Sapporo, Japan) Session 4 - 5.

[85] S.Y. Dai *et al.*, Contrib. Plasma Phys. **56**, 628 (2016).

[86] Z.Q. Hu *et al.*, Nucl. Fusion **54**, 123018 (2014).

[87] Aohua Mao *et al.*, Phys. Plasmas **21**, 052304 (2014).

[88] Aohua Mao *et al.*, Phys. Plasmas **23**, 032117 (2016).

[89] 2nd A3 seminar: NIFS-PROC-92 June 24, 2013.

[90] 3rd A3 seminar: NIFS-PROC-95 December 5, 2013.

[91] 5th A3 seminar: NIFS-PROC-97 October 30, 2014.

[92] 6th A3 seminar: NIFS-PROC-98 December 25, 2015.

[93] 7th A3 seminar: NIFS-PROC-100 July 25, 2016.

[94] 8th A3 seminar: NIFS-PROC-101 September 9, 2016.

[95] 9th A3 seminar: NIFS-PROC-102 January 23, 2017.

[96] 10th A3 seminar: NIFS-PROC-108 January 11, 2018.

[97] 11th A3 seminar: NIFS-PROC-109 January 12, 2018.

[98] 12th A3 seminar: to be published in NIFS-PROC.

[99] 1st A3 A&M seminar: NIFS-PROC-91 February 1, 2013.

[100] 2nd A3 A&M seminar: NIFS-PROC-99 February 1, 2016.

[101] 3rd A3 A&M seminar: NIFS-PROC-103 March 17, 2017.